Theoretical and Applied Fracture Mechanics 143 (2026) 105466

Contents lists available at ScienceDirect

Theoretical and Applied Fracture Mechanics

journal homepage: www.elsevier.com/locate/tafmec

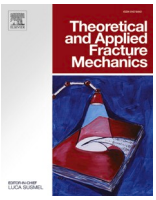

Design net cross-section resistances for numerical design analyses of weakened tensile plates with real material properties

Kirill Golubiatnikov [a,*], Martin Vild [b], Frantisek Wald [a]

[a] Czech Technical University in Prague, Faculty of Civil Engineering, Thakurova 7, 166 29 Prague, Czech Republic
[b] Brno University of Technology, Faculty of Civil Engineering, Veveri 95, 602 00 Brno, Czech Republic

ARTICLE INFO

Keywords:
Finite element analysis
Design net cross-section resistance
Reduction safety factor
Reliability analysis
Structural steel

ABSTRACT

Design net cross-section resistances for numerical design analyses of weakened tensile plates with real material properties have been established. Datasets of possible resistances for each considered geometry type were generated using a Monte Carlo-based procedure, combining a numerical-analytical approach with statistical functions of real material properties and real thicknesses reported in the literature. The generated datasets and the applied numerical - analytical approach were validated against experimental results. Subsequently, the datasets were statistically evaluated in accordance with EN 1990, and design net cross-section resistances with partial safety factors for tensile resistance were determined. The maximum obtained partial safety factor is 1.22, closely matching the recommended value of 1.23 reported in the literature. The most critical geometry types were smooth double notches, round double notches, and either sharp double notches or a narrow slotted hole. Plates with single holes or slotted holes exhibit lower design resistance than comparable double-notch plates. Additionally, staggered holes reduce resistance, whereas multiple holes in line have little effect. The results provide statistically guaranteed criteria suitable for numerical design analyses with real material properties and support harmonization with Eurocode-based practice.

The findings of this study, particularly the derived design resistances, form a foundation for establishing design failure criteria for numerical design calculations performed with nominal material properties and nominal geometry in a future study.

1. Introduction

Elements with weakened cross-sections are widely used in building structures, and their load-bearing capacity remains an important issue [1–3]. The load-bearing capacity depends on material properties, structural geometry, the type of loading, and external conditions. Variations in these factors can lead to changes in rigidity, ductility, and toughness, which in turn may result in different failure modes, such as geometrical, fracture, or plastic instabilities [4].

Geometrical instability, for example buckling, is a typical failure mode for elements primarily subjected to compression [5]. Fracture instability is manifested by brittle fracture initiation [6] or unstable crack propagation in ductile metals [7]. For elements made of structural steel, i.e. with yield strength up to 460 MPa [8], subjected to constant tensile loading, the dominant failure criterion is plastic instability [9]. This type of instability strongly depends on the stress and strain state as well as on boundary conditions [4], and its onset is associated with the initiation of microcracks within the specimen [10]. However, this parameter cannot be directly controlled during a continuous tensile test and plastic instability can be defined by the onset of necking [11], which corresponds to the attainment of the ultimate tensile strength at any point of the weakened cross-section.

In unweakened elements, such as coupon test specimens, the ultimate strength is reached almost simultaneously across the entire cross-section. In contrast, the ultimate strength in weakened elements is reached first at the edge of the weakening due to stress peaks arising from local geometric discontinuities [12], while the remainder of the net cross-section remains in the plastic response. A graphical representation of the failure criterion is shown in Fig. 1.

The vertical axis represents the load, which is more convenient for analytical solutions. The horizontal axis represents the equivalent plastic strain, reflecting the accumulated local plastic deformations throughout the simulation process [13], and is typically employed as a failure criterion in finite element method (FEM) analyses. The onset of necking is defined by the net cross-section resistance N_R and the

* Corresponding author at: Czech Technical University in Prague, Faculty of Civil Engineering, Thakurova 7, 166 29 Prague, Czech Republic.
E-mail addresses: kirill.golubiatnikov@fsv.cvut.cz (K. Golubiatnikov), martin.vild@vutbr.cz (M. Vild), wald@fsv.cvut.cz (F. Wald).

https://doi.org/10.1016/j.tafmec.2026.105466
Received 16 September 2025; Received in revised form 26 December 2025; Accepted 13 January 2026
Available online 22 January 2026

Nomenclature

SCF	stress concentration factor
SCF_{init}	stress concentration factor in the elastic response
$\sigma_{\max}$	maximum local stress
σ_{nom}	nominal stress in the unaffected region
h	depth of the weakening
R	radius of the weakening
N_R	net cross-section resistance
N_R^{Exp}	experimental net cross-section resistance
$N_{\text{R,d}}$	design net cross-section resistance
ε_R	equivalent plastic strain limit
$\varepsilon_{\text{R,d}}$	design equivalent plastic strain limit
ε_u	statistically guaranteed minimum ultimate strain
ε_y	yield strain
ε_sh	hardening strain
A_net	nominal net cross-section area
γ_{M2}	partial safety factor for net cross-section resistance
γ_X	reduction safety factor for design plastic strain limit
f_y, f_u	yield and ultimate strengths
E	young's modulus
μ	mean value
$Stdv$	standard deviation
x_i	individual sample in the dataset
p	number of samples in the dataset
x_d	statistically guaranteed value of the dataset
α	sensitivity factor of the First-order reliability method
β	reliability index for a reference period of 50 years and structural members of class RC2
M	material properties in statistical representation
G	geometry factor
U	uncertainty factor
$f_{N_{\text{R,d}}}\{M,G,U\}$	statistical representation of the design resistance
$f_{\varepsilon_{\text{R,d}}}\{M,G,U\}$	statistical representation of the design strain limit
$\sigma_{\text{eng}}, \varepsilon_{\text{eng}}$	stress and strain in engineering stress - engineering strain format
$\sigma_{\text{true}}, \varepsilon_{\text{true}}$	stress and strain in true stress - true strain format
$f_\text{i}(\mu_\text{i}, Stdv_\text{i})$	statistical representation of parameter i
$t_{\text{real}}, t_{\text{nom}}$	real and nominal thicknesses
w	minimum width of a plate with a single central hole
e_2	transverse edge distance from the hole center to the plate edges
d	hole diameter
$(A_{\text{net}} f_\text{u})$	nominal resistance with perfect nominal geometry

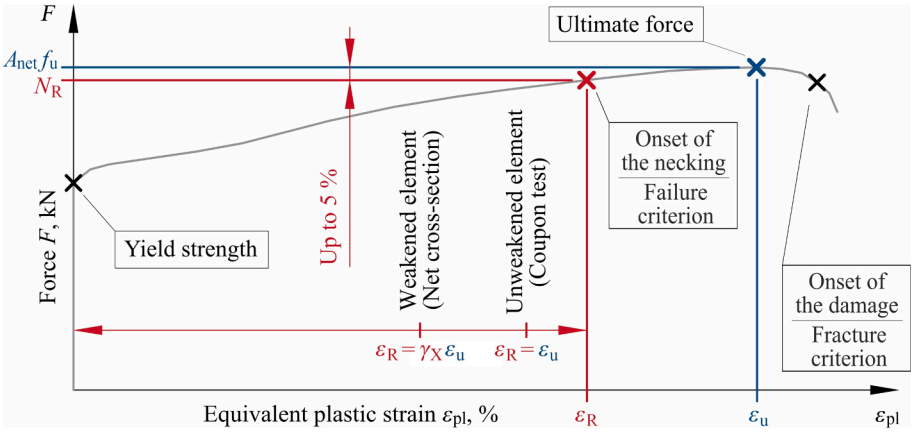

Fig. 1. Graphical representation of the failure criteria for a tensile weakened element, illustrating the onset of necking and fracture.

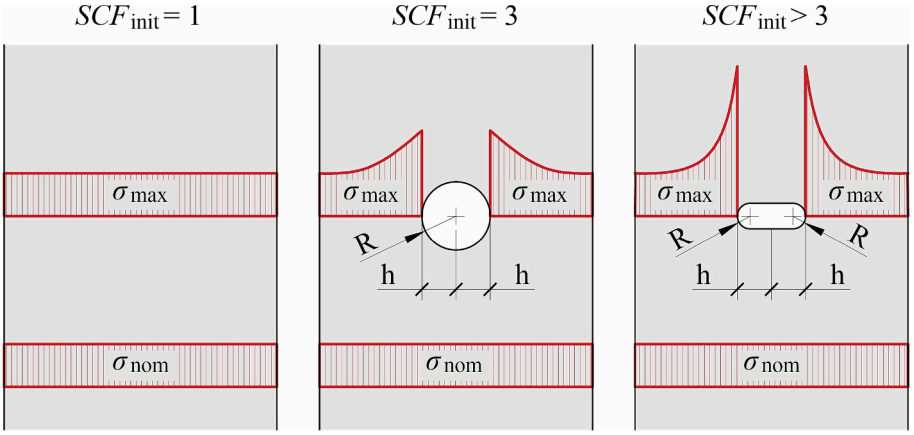

Fig. 2. Examples of stress concentration factor in the elastic response for elements with weakened cross-sections.

equivalent plastic strain limit ε_R.

Local stress peaks in the elastic response have been studied primarily within the framework of elasticity theory [14–17] and in the context of fatigue [18–20]. The magnitude of these peaks depends strongly on the geometry and location of the weakening and is quantified by the stress concentration factor *SCF*, which is expressed as the ratio of the maximum local stress σ_{max}, to the nominal stress σ_{nom} in the unaffected region of the element, as illustrated in several examples in Fig. 2. Murakami [21] proposed a simplified equation to predict the SCF_{init} in the elastic response based on the geometry of the weakening:

$$SCF_{init} = \sigma_{max} \Big/ \sigma_{nom} = 1 + 2\sqrt{h/R} \tag{1}$$

where h is the depth of the weakening and R its radius. The subscript init indicates that this value was determined for the elastic response.

Many studies have examined the stress concentration factor in the elastic response for various geometries of weakened plates. A finite-width plate with a single central hole was reported in [16], and one with an elliptical hole in [22]. Local stress peaks near double-edge notches in both tension and bending plates [23], as well as in cylindrical bars [24], were studied by Nishitani and Noda. The stress concentrations in plates with notches under tension and those with semi-circular notches were presented in [25,26], respectively. The *SCF* for a plate containing a single notch was provided in [27]. Stress fields in specimens with notches under torsion and uniform antiplane shear loading were investigated by Lazzarin et al. [28,29].

The experimental determination of the net cross-section resistance N_R and the equivalent plastic strain limit ε_R for a narrow range of geometrical configurations is possible but the need to use additional tools to measure plastic strain on the specimen surface, such as the digital image correlation method [30]. The common adoption of the ultimate load as the onset of necking is incorrect. Results reported in [17,31,32] show permissible deviations of up to 4.5% in force and inadmissible deviations in strain of up to approximately 30% between these two points.

However, the precise experimental determination of their design values $N_{R,d}$ and $\varepsilon_{R,d}$, which statistically guarantee a probability of occurrence of a lower value of 0.1184% [33], is unrealistic. Achieving this level of statistical confidence would require a wide-ranging tensile testing program, which would be prohibitively expensive. Therefore, the testing program is commonly simplified and limited to extreme cases, and the obtained results are evaluated statistically, for example using the First-order reliability method described in Appendix C of EN 1990 [34]. This approach is presented in **Eq. (2)**, where the analytical expressions of the design failure criteria from FprEN 1993-1-1 [8] and FprEN 1993-1-14 [35] are given on the left-hand side, while the general statistical function $f_i\{M, G, U\}$ of the corresponding parameter is defined on the right-hand side:

$$N_{R,d} = A_{net} f_u \Big/ \gamma_{M2} = f_{N_{R,d}}\{M, G, U\}$$

$$\varepsilon_{R,d} = \gamma_X \varepsilon_u = f_{\varepsilon_{R,d}}\{M, G, U\} \tag{2}$$

Here, A_{net} is the nominal net cross-section area; f_u, ε_u are the ultimate strength and ultimate strain, respectively; γ_{M2}, γ_X are safety factors; M, G denote material and geometry; and U is an uncertainty factor.

The main objective is to define a partial safety factor that guarantees the required probability of 0.1184%. In the 1980s, Snijder et al. evaluated experimental test results of weakened specimens [36] and bolted connections [37]. Based on these findings, the partial safety factor for the net cross-section resistance in tension γ_{M2} was established as 1.25 in the current EN 1993-1-1 [38]. More recently, combined approaches employing both numerical simulations and experimental data have been applied to generate databases. Snijder et al. [33,39] refined γ_{M2} to 1.23, and Sinur and Beg [40] subsequently confirmed this value for cases with the extreme permitted edge distance from the hole center. Može [41,42] investigated the influence of the edge distance on the failure mode of weakened elements, while Hradil and Talja [43] demonstrated that a partial safety factor of $\gamma_{M2} = 1.25$ is statistically sufficient for all steels with an ultimate strain of at least 6%.

By contrast, the reduction safety factor γ_X has been the subject of only limited investigations with a relatively narrow scope [31] [32,44,45], mainly due to the complexity of the testing procedures. The most comprehensive contribution was provided by Solonick [46], who proposed values of γ_X in the range from 0.2 to 0.5 for global, local, or concentrated plastic strain limits.

The improved determination of the safety factor γ_{M2} is a critical issue for the precise design of steel structures and for material savings. This study presents a procedure for determining the design net cross-section resistance of weakened tensile plates with real material properties using the authors' numerical - analytical approach combined with reliability analysis according to EN 1990 [34].

The proposed procedure eliminates the disadvantages of limited experimental tensile testing program, such as considering only extreme cases, and enables the creation of a reliable dataset of structural responses under loading for various combinations of $\{M, G, U\}$. The influence of different variables on the final resistance can thus be analyzed in greater detail. Simultaneously, the use of experimentally validated analytical relationships reduces the number of highly time-consuming numerical simulations. Unlike common data-generation procedures, the proposed approach does not limit the number of samples in the generated datasets. The obtained partial safety factor is compared with the experimentally determined recommended value of 1.23 reported in the literature [33,39], thereby validating the proposed procedure.

The results of this study provide a foundation for establishing a design equivalent plastic strain limit, specifically the reduction safety factor γ_X, for numerical design calculations performed with nominal material properties and nominal geometry in future work.

2. Methodology

The determination of design net cross-section resistance is directly linked to the reliability analysis of a broad dataset of real possible resistances N_R. In this study, the procedure consisted of several main steps:

(1) **Selection of geometrical configurations of weakened tensile plates**

Representative geometry types were defined to cover various stress concentration conditions.

(2) **Experimental analysis**

Static tensile tests were conducted to obtain experimental load – displacement responses and to validate both the numerical - analytical approach and the numerical simulations.

(3) **Determination of individual possible resistance**

A numerical-analytical approach [47] was applied to calculate the possible resistance of each weakened tensile plate based on its material properties, geometry and uncertainty factor.

(4) **Generation of possible resistance and partial safety factor dataset**

A Monte Carlo-based procedure was used to generate large datasets of possible resistances and corresponding safety factors. Material properties and real thickness inputs were defined by statistical functions constrained by European standard conditions. Individual possible resistances were determined by iteratively applying the numerical-analytical approach of three million times. Load - equivalent plastic

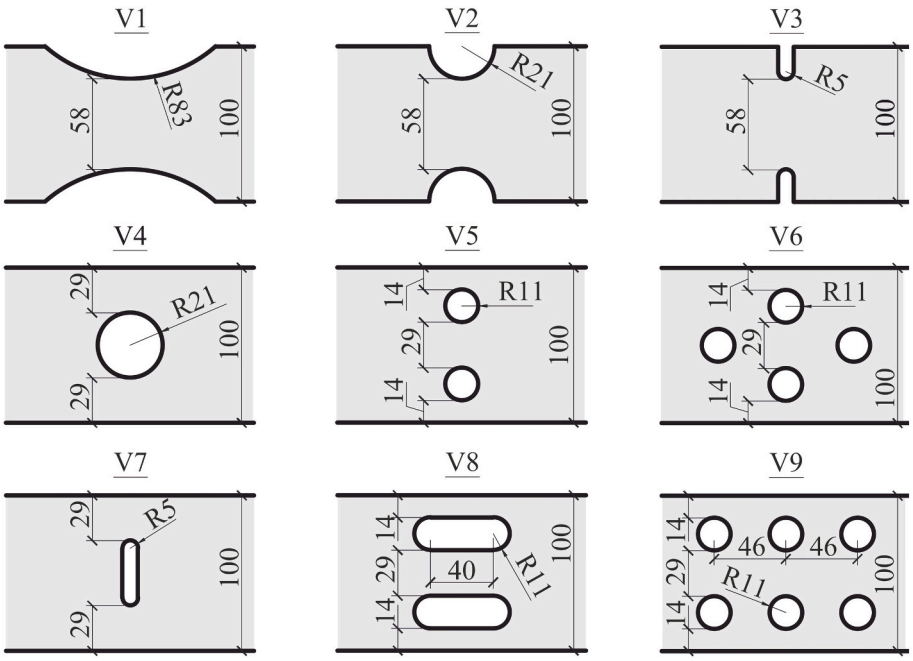

Fig. 3. Geometrical configurations of weakened tensile plates.

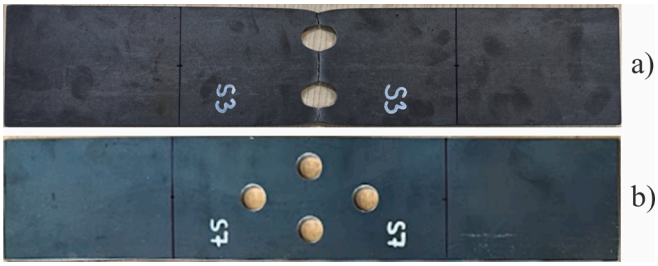

Fig. 4. Weakened specimens prepared for static tensile testing
a) geometry type V5 (after experiment) and b) geometry type V6 (before experiment).

strain responses were obtained through numerical simulations.

(5) Reliability analysis

The datasets were statistically evaluated in accordance with Appendix C of EN 1990 [34] using the First-order reliability method to derive design resistances and partial safety factors γ_{M2} for various geometrical configurations. The analytical equations used to determine the design values in this study are given as follows:

$$\begin{aligned} \mu &= \sum x_i \Big/ p \\ Stdv &= \sqrt{\sum (\mu - x_i)^2 \Big/ (p-1)} \\ x_d &= \mu - \alpha\beta\, Stdv \end{aligned} \tag{3}$$

where, x_i is an individual sample in the assessed dataset, p is the number of samples and x_d is the statistically guaranteed value of the dataset. The coefficients α and β represent the sensitivity factor and the reliability index, respectively, with values of 0.8 and 3.8.

3. Selection of geometrical configurations of weakened tensile plates

A total of nine geometry types with different weakening configurations were considered, specifically double notches, holes, and slotted holes, as illustrated in Fig. 3.

Selected geometrical configurations were designed with the same net cross-sectional area; consequently, their analytical resistances, calculated according to **Eq. (2)**, are identical. All geometry types were defined with the maximum permitted weakening of 41.7%, derived from EN 1993-1-8 [38]. The minimum width w of a plate with a single central hole is equal to twice the transverse edge distance e_2 from the hole center to the plate edges. The minimum permitted edge distance is 1.2 times the hole diameter d. Therefore, the maximum permitted weakening corresponds to 41.7% of the total net cross-section area:

$$w = 2e_2 = 2.4d \rightarrow d = w/2.4 = 0.417w \tag{4}$$

The nominal plate thickness was set to $t_{nom} = 5$ mm, as this nominal thickness exhibits the largest percentage deviations of real to nominal plate thickness t_{real}. These deviations were adopted from the maximum permitted tolerances for hot-rolled steel plates specified in EN 10029 [48].

$$t_{nom} - 0.6\ \text{mm} \le t_{real} \le t_{nom} + 1.2\ \text{mm} \qquad \text{for } 5\ \text{mm} \le t_{nom} < 8\ \text{mm} \tag{5}$$

4. Experimental analysis

In 2024, static tensile tests of weakened specimens, shown in Fig. 4, were conducted at the Faculty of civil engineering of the Brno university of technology. The tested specimens corresponded to geometry types V5 and V6, as defined in Fig. 3. All specimens were cut from a single hot-rolled plate of either S235 or S355 steel with a nominal thickness of 6 mm. The total specimen length was 500 mm, with a width of 100 mm. The gauge length of the observed region was 300 mm, which satisfies the minimum required distance from the machine grips to eliminate the influence of boundary conditions on local stress and strain concentrations [21].

The specimens were fabricated in two stages: preparation of rectangular blanks and drilling of the weakening holes. The blanks were cut by laser with an accuracy of 0.01 mm, and the holes were drilled manually using a standard twist drill. No additional post-processing was carried out.

The real weakening diameters and plate thicknesses were measured

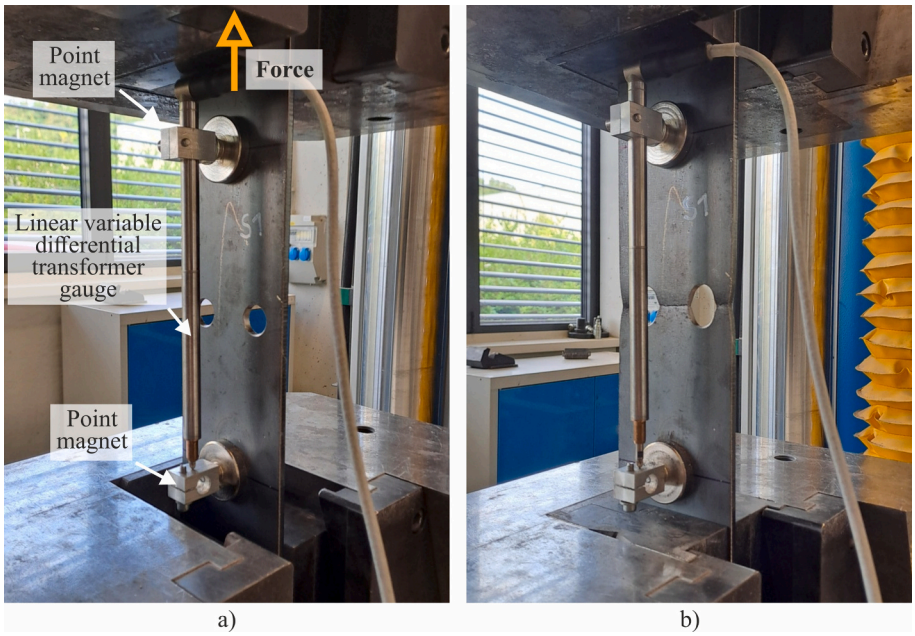

Fig. 5. Measurement layout with gauge rigidly attached to the specimen by point magnets for displacement monitoring a) during the experiment and b) after the experiment.

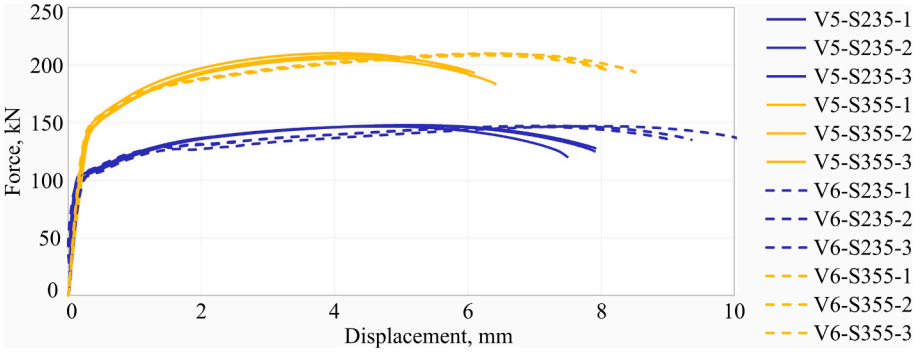

Fig. 6. Experimental load-displacement responses of tested specimens.

at several locations using a digital caliper. The maximum deviation between nominal and real diameter was observed in specimen V5-S355–2 and was equal to 0.23 mm. The largest thickness deviations were found in specimens made of S235 steel. The real weakening diameter statistical distribution was determined as $d_{\text{real}} = f_d(\mu_d = 20.08\ \text{mm}; Sdtv_d = 13.36\%)$ and for the real thickness was $t_{\text{real}} = f_t(\mu_t = 5.85\ \text{mm}; Sdtv_t = 25.63\%)$, calculated according to **Eq. (3)**. Both distributions exhibit significant standard deviations, which are probably caused by the low number of specimens reporting large deviations from the nominal values. Nevertheless, these deviations are still within the permitted tolerances specified in EN 10029 [48], see **Eq. (5)**.

A total of 12 specimens were tested, consisting of six of geometry type V5 and six of geometry type V6. The tests were conducted on a LaborTech testing machine with a maximum force capacity of 1 MN at a constant loading rate of 1 mm/min. Both tensile force and vertical displacement were monitored. The force was recorded directly by the testing machine, while displacement was measured using a linear variable differential transformer gauge with an offset tip rigidly attached to the specimens by point magnets, as shown in Fig. 5. The experimental load - displacement responses are presented in Fig. 6. The responses exhibited a high degree of similarity, particularly up to the attainment of the ultimate force. In all cases, fracture occurred within the net cross-sections.

All measured geometric dimensions, and experimental resistances are summarized in Table 1. The experimental resistance is defined as the maximum force achieved during the static tensile test.

The real material models were determined through coupon tests conducted in accordance with ISO 6892–1:2009 [49]. The coupon specimens were cut from the steel plates during the preparation of rectangular blanks. A total of six specimens were tested: three of steel grade S235 and three of steel grade S355. Each coupon specimen had an overall length of 120 mm and a gauge length of 80 mm. The overall width was 20 mm, reduced to 10 mm in the gauge section. The nominal thickness was 6 mm. The loading rate was set to 1 mm/min. All values were recorded directly by the testing machine.

The resulting material stress-strain curves are presented in Fig. 7. The dashed lines represent individual test results, while the thick solid lines indicate their average values. The yield and ultimate strengths of both steel grades correspond to the recommended mean values obtained from the results of the Safebrictile project [50].

5. Determination of individual possible resistance

The individual resistance of a weakened tensile plate with a defined weakening geometry and a given real thickness was expressed using the numerical-analytical approach from [47] as follows:

Table 1
Measured geometric dimensions and experimental resistances of tested specimens.

Geometry type	Steel grade	Specimen	Real weakening diameter d_{real}	Real thickness t_{real}	Experimental resistance N_R^{Exp}
–	–	–	mm	mm	kN
V5	S235	V5-S235–1	19.94	5.50	146.7
		V5–235-2	20.06	5.49	147.5
		V5-S235–3	20.12	5.54	147.8
	S355	V5-S355–1	20.10	5.95	210.2
		V5-S355–2	20.23	5.95	205.8
		V5-S355–3	20.15	5.83	208.0
V6	S235	V6-S235–1	20.05	5.76	146.4
		V6-S235–2	20.08	5.88	146.9
		V6-S235–3	20.10	5.81	147.2
	S355	V6-S355–1	20.15	6.26	209.6
		V6-S355–2	19.83	6.19	210.1
		V6-S355–3	20.10	6.06	208.3

$$N_R = (A_{net} f_u) G U \tag{6}$$

Here, $(A_{net} f_u)$ notes the nominal resistance of a tensile element with perfect nominal geometry. The geometry reduction factor G reduces this nominal resistance to account for the most unfavorable permitted combination of weakening production deviations. In practice, production deviations are not always at their worst, and the applied manufacturing technology also influences the load resistance. These variations are incorporated into the uncertainty factor U.

Nominal resistances $(A_{net} f_u)$ were determined from load – stress responses under loading by numerical simulations with perfect geometry, employing the linear elastic - linear hardening plastic material model shown in Fig. 8. This material model was chosen because it allows statistically guaranteed strain values to be determined at characteristic points according to **Eq. (7)** for material M with defined yield strength f_y, ultimate strength f_u, and Young's modulus E [34].

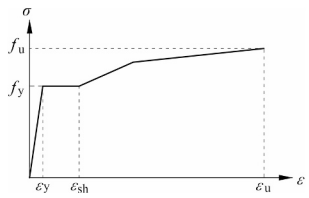

Fig. 8. Linear elastic - linear hardening plastic material model [51].

$$\begin{aligned} \varepsilon_y &= f_y / E \\ \varepsilon_{sh} &= 0.1 f_y / f_u - 0.055 \text{ but } 0.015 \le \varepsilon_{sh} \le 0.03 \\ \varepsilon_u &= 0.6\left(1 - f_y / f_u\right) \text{ but } \varepsilon_u \ge 0.06 \end{aligned} \tag{7}$$

Here, ε_y is the yield strain, ε_{sh} is the hardening strain and ε_u is the ultimate strain. These values are expressed in the engineering stress-engineering strain format, which is typically used in numerical design calculations, since the reduction of cross-sectional area due to the Poisson effect can be neglected in small-displacement solutions [52]. However, numerical simulations must remain valid for all displacement levels, and the reduction of cross-sectional area is considered through conversion of the material model to the true stress - true strain format as follows:

$$\begin{aligned} \sigma_{true} &= \sigma_{eng}\left(1 + \varepsilon_{eng}\right) \\ \varepsilon_{true} &= \ln\left(1 + \varepsilon_{eng}\right) \end{aligned} \tag{8}$$

The geometry is defined by the real thickness, which may differ from its nominal value, and by the accuracy of weakening production. Permitted deviations in the shape and location of weakening for European steel structures are specified in Chapters 6.6 and 6.7 and in Appendix B of EN 1090–2 [53] and are summarized in Fig. 9.

The analytical relationships for the geometry reduction factor G of the selected geometry types were established in [47] based on the results of 198 numerical simulations with varying thicknesses and different permitted combinations of weakening production deviations. The obtained functions were expressed as a function of resistance with respect to the real-to-nominal thickness ratio. For geometry types V2 and V3, the results were subsequently validated against experimental data. The graphical representations of these functions are shown in Fig. 10.

The statistical function of the uncertainty factor U was determined by comparing 178 experimental and numerical - analytical resistance values obtained with $U = 1$. The experimental specimens varied in thickness, manufacturing procedure, and steel grade. The resulting statistical function is presented in **Fig. 11**.

After determination of real possible resistance for random combination of inputs $\{M, G, U\}$, partial safety factor γ_{M2} was calculated as a nominal $(A_{net} f_u)$ resistance to real possible resistance N_R (ratio)

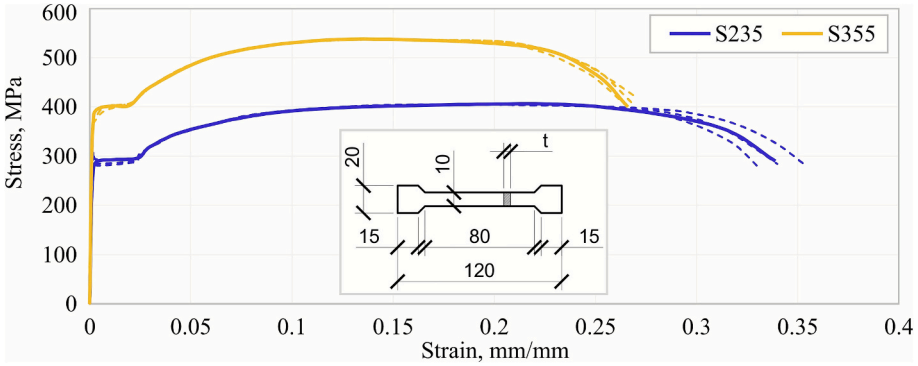

Fig. 7. Stress-strain curves obtained from coupon test results of S235 and S355 steel grades.

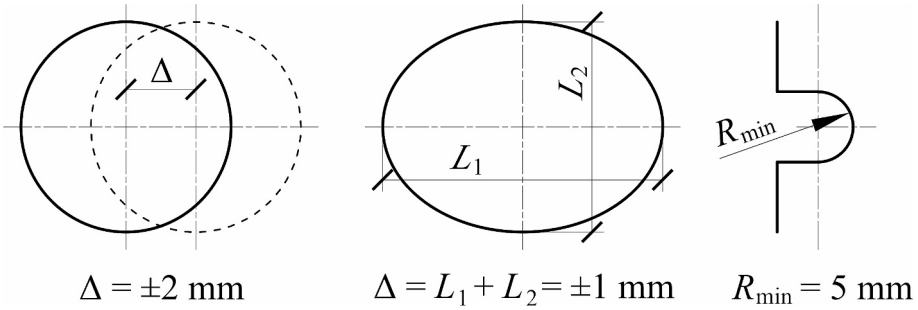

Fig. 9. Permitted deviations in the shape and location of weakening for European steel structures, as specified in EN 1090–2 [53].

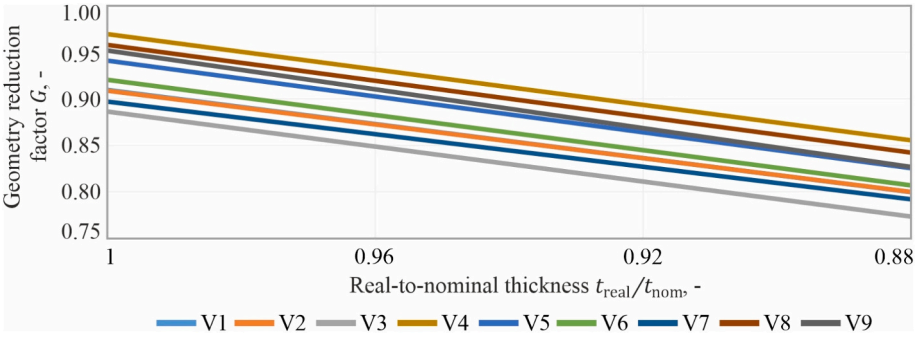

Fig. 10. Geometry reduction factor G as a function of the real to nominal thickness ratio [47].

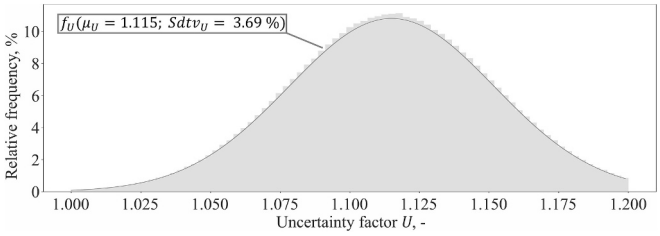

Fig. 11. Relative frequencies of the uncertainty factor U [48].

6. Generation of possible resistance and partial safety factor dataset

6.1. Material properties input

Statistical distributions of individual material properties have been studied in many works [54–56], however the results of the Safebrictile project [50] were adopted in Annex E of FprEN 1993-1-1 [8] and were used in this study. These statistical functions for structural steel, i.e. steel with a yield strength up to 460 MPa, are summarized in Table 2 by mean values μ_i and standard deviations $Stdv_i$. All functions follow a normal distribution. The probability of occurrence of individual values is governed by the density of their original distributions [57]. Therefore, the yield and ultimate strengths are treated as pseudorandom variables.

In addition, European structural steels must satisfy the ductility requirement from [8], expressed as the ratio of yield to ultimate strength limited to $f_u/f_y \geq 1.1$. Young's modulus was taken as a constant value of 210 GPa.

Statistically guaranteed extreme values of the material properties are also presented in Table 2. The yield strength f_y and the ultimate strength f_u were determined according to **Eq. (3).** with a reliability index $\alpha\beta$ of ±3.04. The minimum f_u/f_y ratio corresponds to the ductility requirement, while the maximum ratio was calculated using the extreme opposite values of strengths. The ultimate strains were determined according to **Eq. (7)** based on the same extreme values.

Table 2
Statistical parameters and guaranteed extreme values of yield strength, ultimate strength, ultimate-to-yield strength ratio and ultimate strain.

		Yield strength f_y, MPa	Ultimate strength f_u, MPa	Ultimate-to-yield strength f_u/f_y, –	Ultimate strain ε_u, mm/mm
S235	Mean value	294	432		
	Standard deviation	16.2	21.6		
	Minimum	244.84	372.90	1.1	0.06
	Maximum	343.16	491.10	2.01	0.30
S355	Mean value	426	529		
	Standard deviation	21.3	21.2		
	Minimum	361.25	476.73	1.1	0.06
	Maximum	490.75	581.27	1.61	0.23
S460	Mean value	529	594		
	Standard deviation	23.8	20.8		
	Minimum	456.73	535.31	1.1	0.06
	Maximum	601.37	652.69	1.43	0.18

Material properties, represented by three million pseudorandom pairs of yield and ultimate strengths, were generated from statistical functions constrained by the ductility requirement, as illustrated in Fig. 12a). Performing such a large number of simulations is computationally demanding; therefore, the possible yield and ultimate strengths for each steel grade were grouped according to their f_u/f_y ratios based on standard mathematical classification rules. Relative frequencies were then established for each group, as shown in Fig. 12b). Six ratio groups -

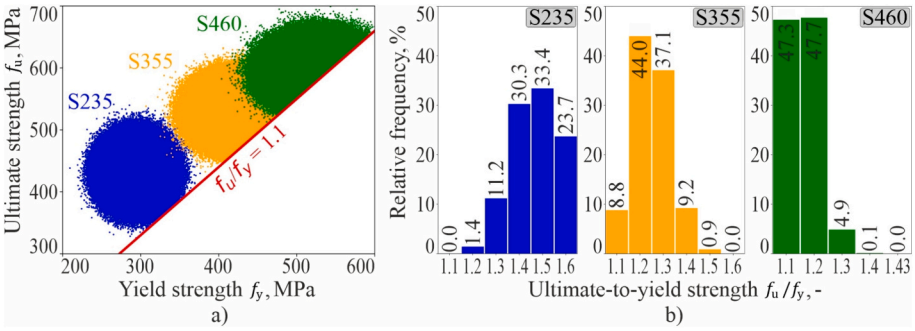

Fig. 12. Possible material properties for European structural steels
a) real representation and b) simplified representation.

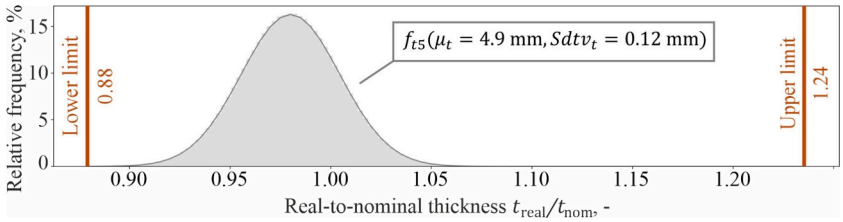

Fig. 13. Relative frequencies of the real-to-nominal thickness ratio for a nominal thickness of 5 mm.

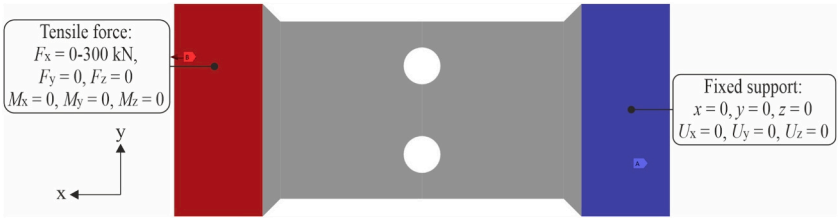

Fig. 14. Example of boundary conditions applied in the numerical simulations, geometry type V5.

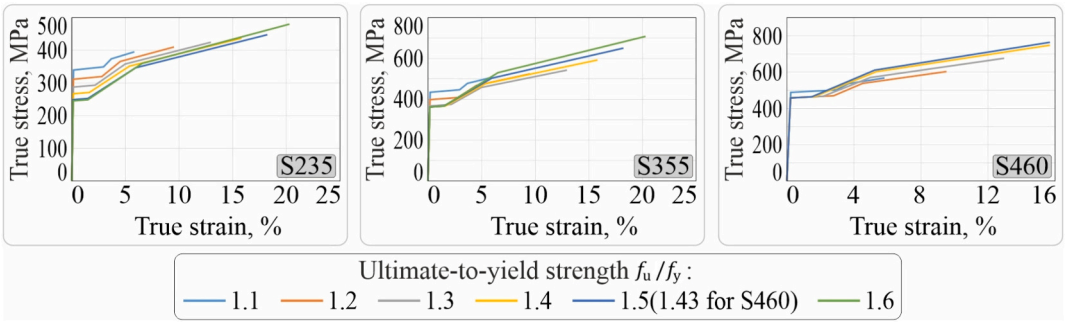

Fig. 15. Material models applied in the numerical simulations of the simplified representation of S235, S355, and S460 steel grades from Fig. 12a) in the true stress-true strain format.

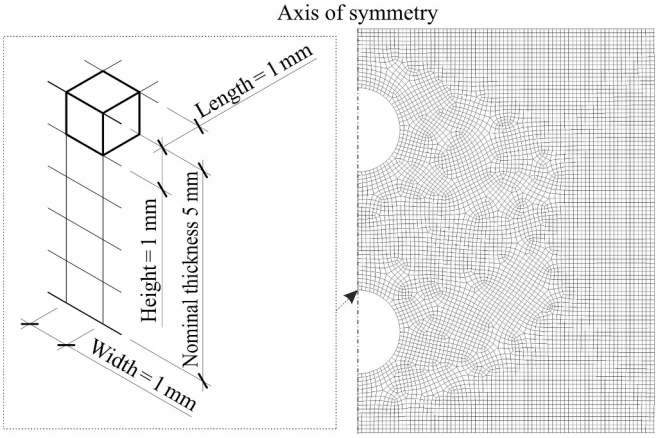

Fig. 16. Finite element mesh of the numerical specimen generated with 20-node cubic elements and a uniform element size of 1 mm, geometry type V5.

1.1, 1.2, 1.3, 1.4, 1.5, and 1.6 - were defined for the S235 and S360 steel grades. Ratios larger than 1.6 were treated as 1.6. For the S460 steel grade, only five groups were defined, with a maximum ratio of 1.43.

6.2. Real thickness input

The real thickness t_{real} of a tensile element may differ from its nominal value and depends on both the type of structural element and the measurement location. The largest deviations are typically observed in the flange thicknesses of I- and H-profiles, [50,58]. The statistical function describing the distribution of real thicknesses is presented in Fig. 15 and follows a normal distribution. The maximum permitted deviations for hot-rolled steel plates are specified in EN 10029 [48] and are expressed in **Eq. (5)**. These tolerance limits were adopted as the boundaries for the real thickness values.

6.3. Numerical simulations

The numerical simulations were performed in Ansys 2022 R2 using the Static structural analysis system. All simulations were carried out as static tensile tests up to the onset of necking, corresponding to the force at which the ultimate strength was attained at least at one point. One end of the numerical specimen was fully constrained (fixed support), preventing displacements and rotations, while a longitudinal tensile force was applied at the opposite end. An example of the boundary conditions for geometry type V5 is shown in Fig. 14. The numerical specimen had an overall length of 500 mm, a gauge length of 300 mm, and a gauge width of 100 mm, with widened ends of 140 mm. The thickness was set to 5 mm.

Simulations with numerical specimens for each geometry type were performed using material models in true stress–true strain format, corresponding to simplified representations of the S235, S355, and S460 steel grades shown in Fig. 12. The engineering material models were determined according to **Eq. (7)**, using the statistically guaranteed minimum ultimate strengths f_u from Table 2 and the yield strength f_y, calculated based on the required ultimate-to-yield strength ratio. If the calculated yield strength fell outside the range of statistically guaranteed extreme values, the models were instead defined by the minimum yield strength, with the ultimate strength calculated to satisfy the required ratio. The material properties obtained in this manner represent statistically guaranteed minimum values for each f_u/f_y ratio. The linear elastic - linear hardening plastic model defines statistically guaranteed minimum strains [51]. Accordingly, the resulting engineering material

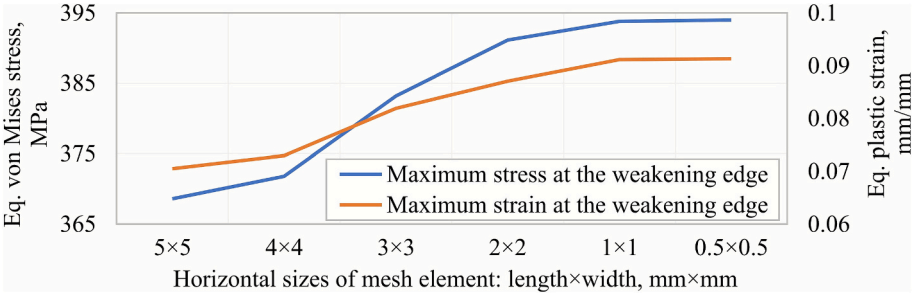

Fig. 17. Mesh sensitivity study for geometry type V3 [47].

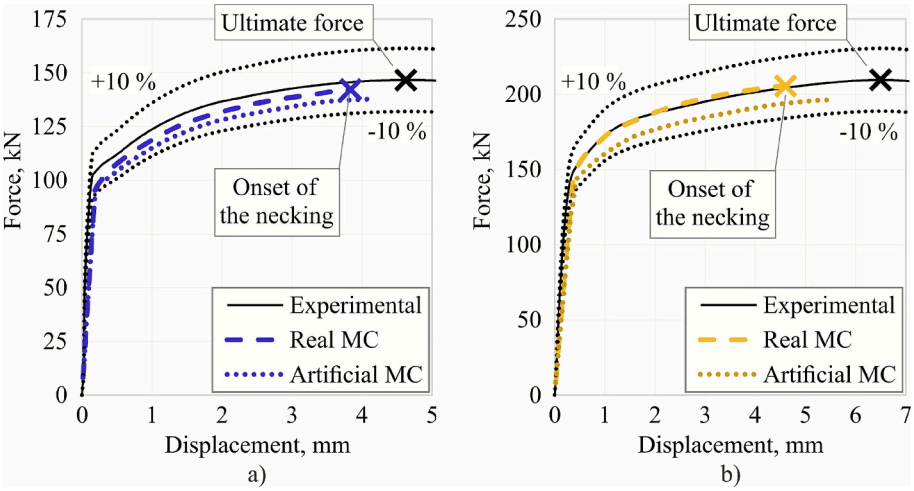

Fig. 18. Experimental and numerical load-displacement responses for specimens a) V5-S235–1 and b) V6-S355–1.

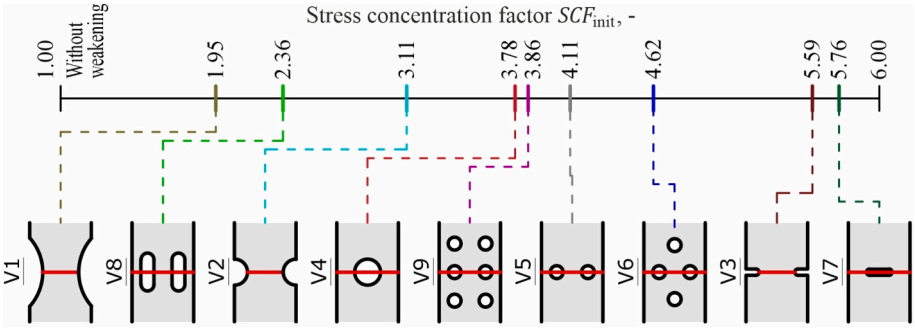

Fig. 19. Numerically determined stress concentration factor SCF_{init} in elastic response at the weakening edge of the net cross-section (red line). (For interpretation of the references to colour in this figure legend, the reader is referred to the web version of this article.)

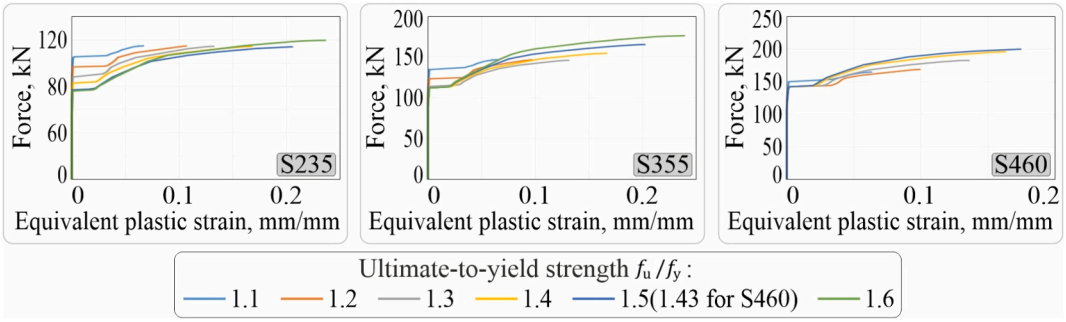

Fig. 20. Example of numerically determined load - equivalent plastic strain responses for geometry type V1.

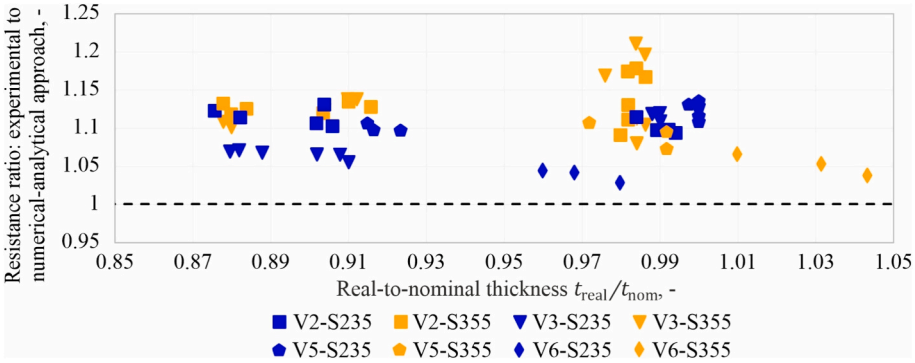

Fig. 21. Ratios of experimental to predicted resistances for geometry types V2 and V3 from [47] and V5 and V6 from this study.

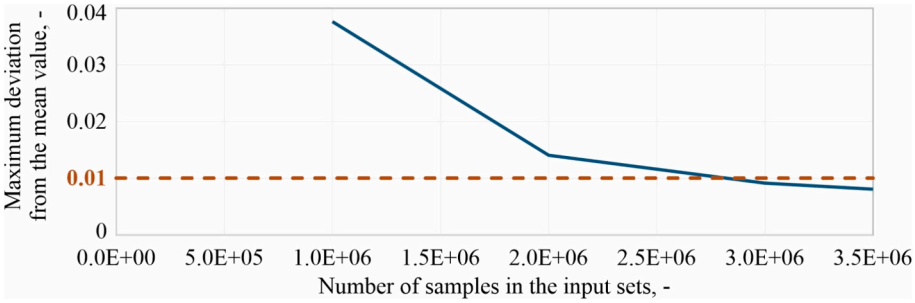

Fig. 22. Results of the sensitivity study for geometry type V3 made of S235 steel.

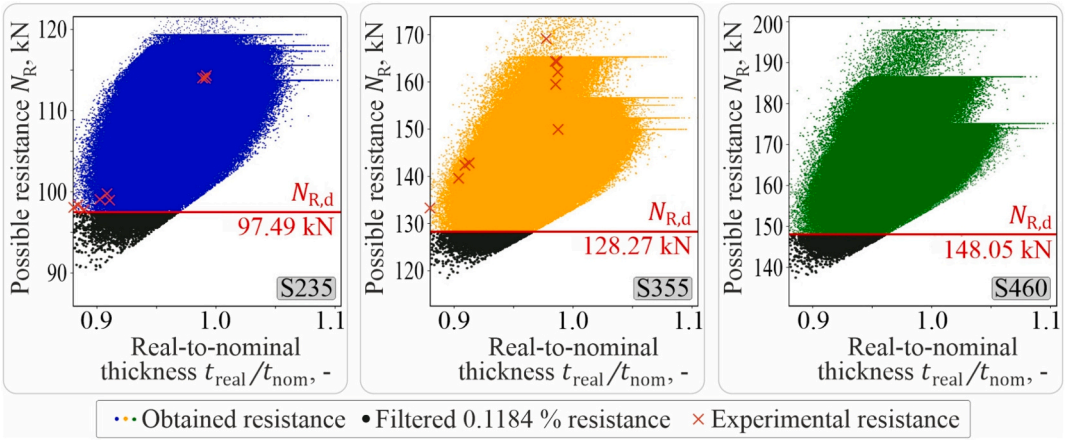

Fig. 23. Determination of design resistance for geometry type V3 and comparison with experimental resistances from [47].

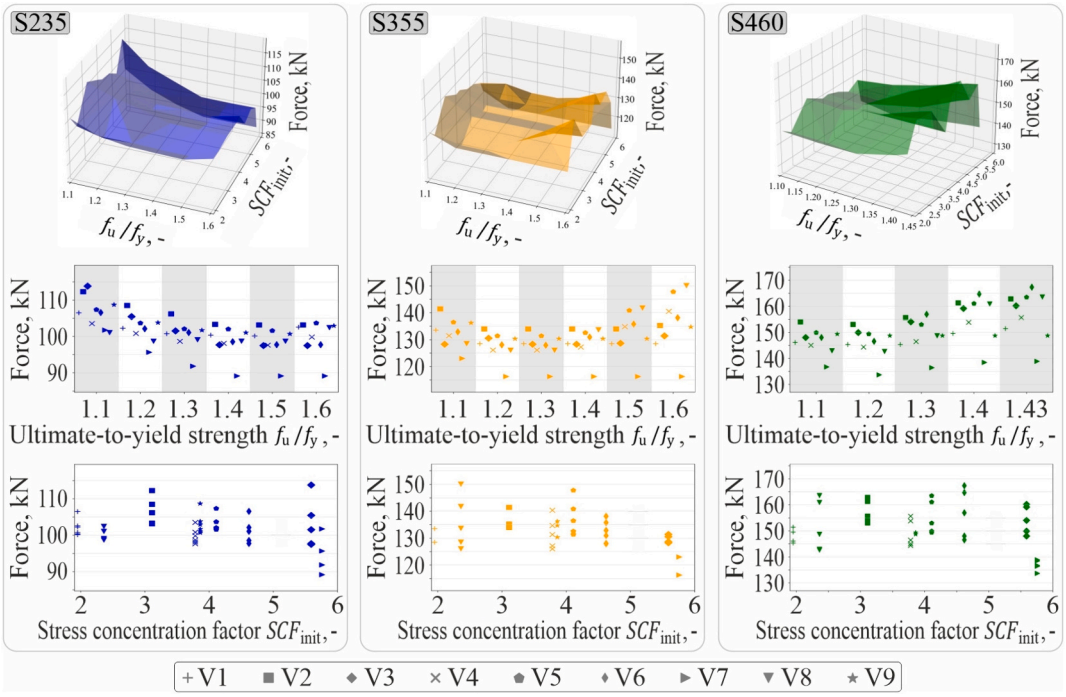

Fig. 24. Summary of design resistances by geometry type, categorized by the ultimate-to-yield strength ratio f_u/f_y and the stress concentration factor SCF_{init} in the elastic response.

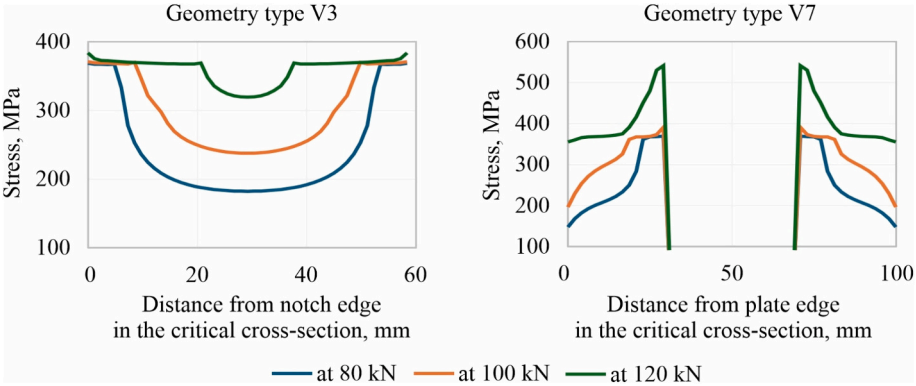

Fig. 25. Stress distributions in the critical cross-section of geometry types V3 and V7, indicated by the red line in Fig. 19, at various load levels in the plastic response. (For interpretation of the references to colour in this figure legend, the reader is referred to the web version of this article.)

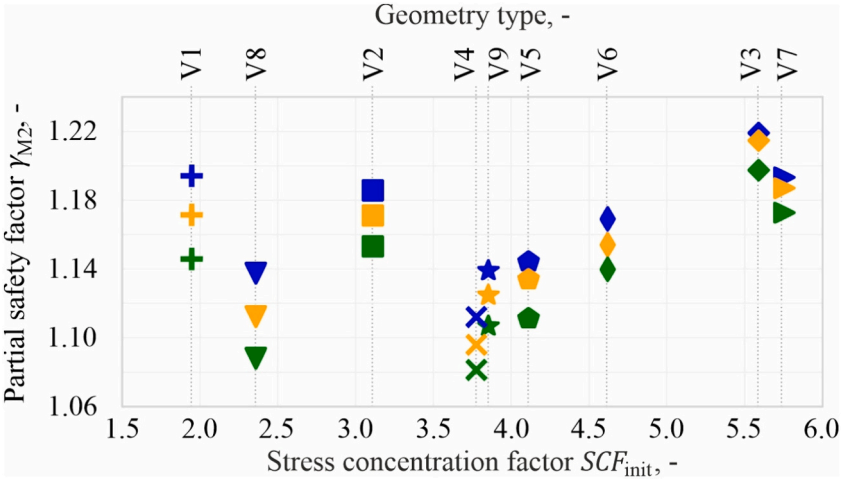

Fig. 26. Partial safety factors γ_{M2} across geometry types and steel grade of S235 (blue), S355 (orange) and S460 (green). (For interpretation of the references to colour in this figure legend, the reader is referred to the web version of this article.)

models represent the statistically guaranteed strain minima for each steel grade and required f_u/f_y ratio. These models were then converted into the true stress–true strain format and are presented in Fig. 15.

The Isotropic elasticity and Multilinear isotropic hardening material tools were used in Ansys to define the material behavior. Elastic modulus was set to 210 GPa and Poisson's ratio to 0.3. Nonlinear plastic deformation was described by a stress-plastic strain table, starting at the yield strength with zero plastic strain.

The numerical modeling procedure was adopted from the numerical-analytical approach [47], where they had been validated by comparing experimental and numerical load - displacement responses, showing deviations in resistance of up to 7%. The numerical mesh was generated using 20-node cubic elements (SOLID186) with a uniform element size of 1 mm in all directions, as illustrated in Fig. 16.

The recommended mesh parameters were determined through a sensitivity study on geometry type V3 in [47], which produces the highest local stress and strain peaks; therefore, even small changes were clearly observable. The maximum stress and equivalent plastic strain at the weakening edges were evaluated under a load of 100 kN. The mesh element height was kept constant at $0.2t_{nom}$, i.e. 1 mm. The results, presented in Fig. 17, show that both parameters stabilized and remained nearly constant for mesh sizes of 1 mm × 1 mm and finer.

The numerical modeling procedure was validated against the experimental results for specimens V5-S235–1 and V6-S355–1 from this study. The geometry of the numerical specimens was identical to that of the tested specimens, including the real thickness and weakening diameters. Numerical simulations were performed using the real material model (Real MC) obtained from the coupon tests shown in Fig. 7, as well as an artificial material model. The artificial material model (Artificial MC) represented the linear elastic-linear hardening plastic material model from Fig. 8 calibrated with the real material properties obtained from the coupon tests.

The experimental and numerical load-displacement responses are presented in Fig. 18. Both simulations reproduced the experimental results with high accuracy. The numerical simulation with the Real MC model underestimated the net cross-section resistance by up to 2.9%, while the simulation with the Artificial MC model deviated by up to 6.3%. Although the Artificial MC simulations are more conservative, their accuracy remains sufficiently high.

A total of 153 simulations were performed. Firstly, the stress concentration factor SCF_{init} in the elastic response were determined numerically for each geometry type to distinguish their behavior, which was calculated as the ratio of the maximum stress at the weakening edge of the net cross-section to the nominal stress measured at the mid-width of the plate, 100 mm away from the weakening. The obtained values are presented in Fig. 19. The selected geometry types cover the majority of the broad range between uniaxial and biaxial local stress states.

The main results of the numerical simulations were load - equivalent plastic strain responses, obtained for each combination of geometry type, steel grade, and ultimate-to-yield strength ratio. The load, or tensile force, was defined as the applied force, while plastic strains were measured at the weakening edge of the net cross-section, i.e. at the local strain peak. An example of these responses for geometry type V1 is shown in Fig. 20. These responses were subsequently used to generate a reliable and wide-ranging dataset of possible resistances N_R for each geometry type.

6.4. Monte Carlo simulation

The datasets were generated using a Python 3.10 script in Visual Studio Code, following an approach analogous to Monte Carlo simulation. Input sets of possible ultimate-to-yield strength ratios, real thicknesses, and uncertainty factors were generated independently as pseudorandom parameters, i.e. the probability of occurrence of each value followed its original statistical function and limiting condition. All sets contained the same number of samples. Once a geometry type was selected, one f_u/f_y ratio and randomly corresponding values of thickness t_{real} and uncertainty factor U were assigned to determine an individual possible resistance N_R using the numerical-analytical approach, as expressed in **Eq. (6)**. The relevant load - equivalent plastic strain response was selected from the set of numerically determined responses, and the nominal resistance of a tensile element with perfect geometry $(A_{net}f_u)$ was established. The geometry reduction factor G was calculated based on the geometry type and the ratio of real to nominal thickness, as shown in Fig. 10. Finally, the nominal resistance was multiplied by the geometry reduction factor and the uncertainty factor to obtain the possible resistance N_R. The partial safety factor γ_{M2} were calculated by dividing the obtained resistance by the nominal resistance for each considered combination of $\{M, G, U\}$, the latter determined according to **Eq. (2)**. The four resulting values were then stored in their respective datasets. The entire numerical-analytical procedure was applied to all randomly generated combinations of f_u/f_y ratios, real thicknesses t_{real} and uncertainty factors U.

Validation of the numerical-analytical approach and of the number of samples in the input sets was a crucial step of the procedure. Validation was carried out by comparing experimental resistances with possible resistances determined according to **Eq. (6)**. Experimental resistances and real material properties were taken for geometry types V2

and V3 from [47] and from the experimental analysis in this study. Nominal resistances $(A_{net}f_u)$ were calculated using numerical simulations with the linear elastic - linear hardening plastic material model combined with real material properties obtained from coupon tests. Possible resistances N_R were determined using an uncertainty factor of 1. The ratios of experimental to predicted resistance are shown in Fig. 21. All ratios exceed 1.0, with the majority of values clustering around 1.1, corresponding to the mean value of the uncertainty factor U.

The required number of samples was determined by a sensitivity study on the design net cross section resistance $N_{R,d}$ for geometry V3 of S235 steel grade, which produces the largest local stress peak, similarly to the right example shown in Fig. 2. Input sets were generated for selected sample numbers, and dataset of possible real resistances N_R was obtained using the numerical - analytical approach. The lowest 0.1184% of possible resistances were excluded, and the last remaining value was taken as $N_{R,d}$. Each procedure was repeated ten times per sample size, and deviations from the mean were evaluated according to **Eq. (3)**.

The target of a maximum deviation of 0.01 was obtained with around 2.8 million samples in input sets and rounded to three million in this study, as presented in Fig. 22.

Finally, input sets were generated with three million samples each. The input set of possible ultimate-to-yield strength ratios f_u/f_y, presented in Fig. 12, was created as a pseudorandom parameter based on the statistical function and ductility requirement given in Table 2. The distribution of possible real thicknesses t_{real} followed the statistical function given in [58] and the maximum permitted deviations specified in EN 10029 [48], and is presented by the relative frequencies shown in Fig. 13. The probability distribution of uncertainty factor U was taken directly from the original function in **Fig. 11** (thick black line), within the range 1.00 to 1.20 and using a step size of 0.01.

All three input sets were generated independently, resulting in random combinations of material properties, geometry, and weakening production accuracy. Consequently, possible resistances N_R were generated as random values in accordance with the rules of Monte Carlo simulation. An example of the generated resistances for geometry type V3 with all considered steel grades is shown Fig. 23, where colored dots represent the simulated results. Dark red crosses indicate experimental resistances of specimens with various combinations of permitted deviations from [47]. Experimental specimens were produced with three thicknesses: 5 mm, 4.55 mm, and 4.4 mm. The last thickness represents the lowest permitted deviation from the nominal thickness of 5 mm. In addition, specimens made of S355 steel exhibited porous defects, which increased the scatter of the measured values.

The lowest possible resistances in all generated datasets form oblique lower bounds against the ratio of real to nominal thickness depended on bounds arising from the material ductility requirement of 1.1. Possible resistances with the same values but various thickness ratios represent the nominal resistances $(A_{net}f_u)$, obtained from numerical simulations with perfect geometry. If a calculated possible resistance exceeded the nominal resistance, the nominal value was adopted.

At the same time, datasets of the partial safety factor γ_{M2} were calculated as the ratio of the nominal resistance $(A_{net}f_u)$, defined as the maximum resistance in the load - equivalent plastic strain responses in Fig. 20, to the real possible resistance N_R for each random combination of input values $\{M, G, U\}$.

7. Reliability analysis

The dataset of possible resistance for each selected geometry type were statistically evaluated to establish design net cross-section resistance in accordance with EN 1990 [34]. The permitted probability of occurrence below the design value is 0.1184% ($\alpha\beta = 3.04$). The design criterion was therefore defined as the lowest value after excluding 0.1184% of outcomes. Fig. 23 illustrates the procedure for geometry type V3: colored dots represent possible resistances relative to the thickness ratio, dark gray dots mark the filtered values, and the red line indicates the guaranteed design resistance.

Obtained design resistances are summarized in Fig. 24, categorized by the strength ratio f_u/f_y and the stress concentration factor SCF_{init} in the elastic response. The lowest design resistances, normalized by f_u/f_y, inversely follow the frequency distribution of steel grades in Fig. 12: more frequent ratios yield lower resistances. This reflects the interaction of the generation process and reliability analysis, which applies less stringent criteria to rare ratios.

Grouping by SCF_{init} factors show no major dependence, only almost negligible reducing with increasing of stress concentration factor. However, comparison of geometry types V2 vs. V4, V3 vs. V7, which have similar weakening in the critical cross-section but differ in their locations, shows that a single weakening – such as a central or slotted hole - reduces the resistance more than double notches. This effect is caused by stress redistribution during the plastic response in the critical net cross-sections, indicated by the red lines in Fig. 19.

In geometries with notches, stresses in the critical section gradually increased, with the plastic zone slowly expanding from the notch edge inward. After approximately 75% of the cross-section had plasticized, a local stress peak started to form at the notch edge, as shown in the left image of Fig. 25. In contrast, in geometries with a single internal weakening, a local stress peak appeared almost immediately after the onset of plasticity, restricting the effective use of the entire cross-section, as shown in the right image of Fig. 25. Consequently, the ultimate strength in the geometries with holes was reached locally earlier, and the resistance was about 12.2 % lower.

Geometry types with several internal holes exhibit nearly identical resistances, but type V6, with staggered holes, shows slightly lower resistance than the corresponding types V5 and V9.

This behavior corresponds to the trends observed in the geometry reduction factor G, indicating that permitted deviations in the shape and location of the weakening lead to larger local changes in the stress field for the geometry type with staggered holes.

In both cases, the differences in resistance were caused by different redistributions of the stress field within the critical weakened cross-section during the plastic response. These redistributions resulted in different local stress peaks, which can be described by a stress concentration factor in the plastic response rather than in the elastic response. In real steel elements, higher local stress peaks promote increased microcrack initiation, which subsequently leads to a faster onset of plastic instability.

Subsequently, the partial safety factor factors corresponding to 0.1184% of the lowest possible resistances in Fig. 23 were also filtered out. The maximum remaining value was accepted as design partial safety factor γ_{M2} for each considered geometry type, presented in Fig. 26. The maximum γ_{M2} was 1.22 for V3, consistent with the recommended 1.23 [33,39].

Safety factors vary with steel grade and the frequency of f_u/f_y ratios: a wide scatter (S235) increases resistance variability N_R, requiring larger reductions by γ_{M2}. These patterns distinguish structural from high-strength steels, where lower ratios mean local fracture may precede ultimate strength.

The most critical geometry types are V1, V2, and either V3 or V7. The absolute values of the design resistances primarily depend on the nominal ultimate resistance $A_{net}f_u$, which reflects the stress redistribution capacity of the weakened tensile plate. Additionally, they inversely follow the distribution of the relative frequencies of the f_u/f_y ratios within each steel grade. The partial safety factor γ_{M2} was found to be sensitive to the permitted geometrical tolerances.

8. Conclusion

This study established design net-section resistances for plates subjected to static tensile loading with stress concentrators, incorporating

real material properties. Datasets of possible resistances N_R were generated using a Monte Carlo-based procedure that combined hybrid numerical - analytical approach with statistical distributions of real material properties and plate thicknesses reported in the literature. The generated datasets and the applied numerical – analytical approach were validated against experimental results. Subsequently, the datasets were statistically evaluated in accordance with EN 1990, and design net-section resistances $N_{R,d}$ together with partial safety factors γ_{M2} were determined for each geometry type.

The main conclusions are as follows:

- The proposed Monte Carlo-based procedure offers an efficient alternative to extensive tensile testing programs or large-scale numerical simulations,
- The maximum obtained partial safety factor, $\gamma_{M2} = 1.22$, is in excellent agreement with the recommended value of 1.23 proposed by Snijder et al. [33,39],
- The resistance of weakened tensile plate is depended on stress concentration factor in plastic response, which explained stress redistribution in critical cross-section,
- The resistance of a weakened tensile plate depends on the stress concentration factor in the plastic response, which reflects the stress redistribution in the critical cross-section,
- Plates with a single internal discontinuity, such as a hole or slotted hole, exhibited lower resistance than comparable double-notch configurations,
- The number of holes aligned along the same longitudinal axis had little influence on resistance, whereas staggered holes reduced it significantly,
- The most critical geometries were V1 (smooth double notches), V2 (round double notches), and either V3 (sharp double notches) or V7 (narrow slotted hole).

Numerical design calculations are performed using statistically defined nominal material properties recommended in FprEN 1993-1-1, which are generally more conservative than the real properties considered in this study. Furthermore, the adopted numerical modeling approach may influence local stress and strain concentration. The results presented here, particularly the derived design resistances, provide a solid foundation for establishing design failure criteria applicable to numerical design calculations based on nominal material and geometric parameters in future work.

CRediT authorship contribution statement

Kirill Golubiatnikov: Writing – original draft, Visualization, Validation, Methodology, Formal analysis, Conceptualization. **Martin Vild:** Writing – review & editing, Project administration, Methodology, Formal analysis, Conceptualization. **Frantisek Wald:** Writing – review & editing, Supervision, Project administration, Methodology, Formal analysis, Conceptualization.

Declaration of competing interest

The authors declare the following financial interests/personal relationships which may be considered as potential competing interests: Frantisek Wald reports financial support was provided by Ministry of Education, Youth and Sports of the Czech Republic. If there are other authors, they declare that they have no known competing financial interests or personal relationships that could have appeared to influence the work reported in this paper.

Acknowledgement

The study was supported by a project of the Ministry of Education, Youth and Sports of the Czech Republic, Inter Excellence LUAUS23114.

Data availability

Data will be made available on request.

References

[1] A. Torabi, Estimation of tensile load-bearing capacity of ductile metallic materials weakened by a V-notch: the equivalent material concept, Mater. Sci. Eng. A 536 (2012) 249–255, https://doi.org/10.1016/j.msea.2012.01.007.
[2] S. Afkhami, E. Dabiri, K. Lipiäinen, H. Piili, T. Björk, Effects of notch-load interactions on the mechanical performance of 3D printed tool steel 18Ni300, Addit. Manuf. 47 (2021) 102260, https://doi.org/10.1016/j.addma.2021.102260.
[3] R. Dalcin, L. Nicolini, J. Preichardt, C. Scheuer, R. Lermen, I. Machado, Static bending behavior of welded connections between columns-to-beam square hollow sections in Strenx700MC high-strength steel, J. Mater. Eng. Perform. 34 (20) (2025), https://doi.org/10.1007/s11665-025-12341-9.
[4] A. Pineau, A. Benzerga, T. Pardoen, Failure of metals I: brittle and ductile fracture, Acta Mater. 107 (2016) 424–483, https://doi.org/10.1016/j.actamat.2015.12.034.
[5] J. Han, W. Xie, W. Zhang, L. Yang, Adaptive damage analysis method for ultimate bearing capacity of steel truss structures with box section, Sci. Rep. 15 (2025) 8957, https://doi.org/10.1038/s41598-025-93307-8.
[6] S. Souguir, L. Brochard, K. Sab, Stress concentration and instabilities in the atomistic process of brittle failure initiation, Int. J. Fract. 224 (2020) 235–249, https://doi.org/10.1007/s10704-020-00459-x.
[7] S. Cicero, T. García, V. Madrazo, I. Carrascal, E. Ruiz, Analysis of notch effect in load bearing capacity, apparent fracture toughness and fracture micromechanisms of ferritic–pearlitic steels, Eng. Fail. Anal. 44 (2014) 250–271, https://doi.org/10.1016/j.engfailanal.2014.05.007.
[8] FprEn 1993-1-1, *Design of steel structures — Part 1–1: General rules and rules for buildings.* Berlin, 2024.
[9] Y. Bao, T. Wierzbicki, On fracture locus in the equivalent strain and stress triaxiality space, Int. J. Mech. Sci. 46 (1) (2004) 81–98, https://doi.org/10.1016/j.ijmecsci.2004.02.006.
[10] V. Tvergaard, Material failure by void growth to coalescence, Adv. Appl. Mech. 27 (1989) 83–151, https://doi.org/10.1016/S0065-2156(08)70195-9.
[11] C. Li, E. Daxin, N. Yi, Analysis on fracture initiation and fracture angle in ductile sheet metal under uniaxial tension by experiments and finite element simulations, J. Mater. Res. 31 (24) (2016) 3991–3999, https://doi.org/10.1557/jmr.2016.412.
[12] E. Niemi, W. Fricke, S. Maddox, The Structural Hot-Spot Stress Approach to Fatigue Analysis of Welded Components. Designer's Guide, Second edition, Springer, Singapore, 2018 (ISBN 978-981-10-8686-9.).
[13] J. Zheng, X. Shu, Y. Wu, H. Xu, Q. Lu, B. Liao, B. Zhang, Investigation on the plastic deformation during the stamping of ellipsoidal heads for pressure vessels, Thin-Walled Struct. 127 (2018) 135–144, https://doi.org/10.1016/j.tws.2018.01.040.
[14] G. Glinka, Cyclic plasticity applied to the notch analysis of metals, in: Cyclic plasticity of metals: Modeling fundamentals and applications, 2022, pp. 283–323, https://doi.org/10.1016/B978-0-12-819293-1.00019-X.
[15] S. Timoshenko, J. Goodier, Theory of Elasticity, *Third edition.* [Art], McGraw-Hill, London, 1970.
[16] R. Howland, On the stresses in the neighbourhood of a circular hole in a strip under tension, Phil. Trans. R. Soc. A (1930) 49–86, https://doi.org/10.1098/RSTA.1930.0002.
[17] P. Studer, A. Taras, Experimental and simulation data of hole bearing type connections, Data Brief 53 (2024) 110127, https://doi.org/10.1016/j.dib.2024.110127.
[18] A. Hobbacher, Recomendations for fatigue design of welded joints and components, Second edition, Springer International Publishing Switzerland, 2016, https://doi.org/10.1007/978-3-319-23757-2_4.
[19] A. Chattopadhyay, G. Glinka, M. El-Zein, J. Qian, R. Formas, Stress analysis and fatigue of welded structures, in: Welding In The World 55, 2011, pp. 2–21, https://doi.org/10.1007/BF03321303.
[20] K. Golubiatnikov, F. Wald, Stress range in the welded cruciform joint in the shell model using the Hot Spot Stress Method, Eurosteel 6 (3–4) (2023) 2463–2467, https://doi.org/10.1002/cepa.2374, ce/papers.
[21] Y. Murakami, Theory of Elasticity and Stress Concentration, Wiley, Hoboken, 2017. ISBN 978–1–119-29513-6.
[22] M. Isida, On the tension of a strip with a central elliptic hole (part II), Trans. Japan Soc. Mech. Eng. 107 (1955) 507–513, https://doi.org/10.1299/kikai1938.21.507.
[23] H. Nisitani, N. Noda, Stress concentration of a strip with double edge notches under tension or in-plane bending, Eng. Fract. Mech. 23 (1986) 1051–1065, https://doi.org/10.1016/0013-7944(86)90147-5.
[24] H. Nisitani, N. Noda, Stress concentration of a cylindrical bar with a V-shared circumferential groove under torsion, tension or bending, Eng. Fract. Mech. 20 (1984) 743–766, https://doi.org/10.1016/0013-7944(84)90084-5.
[25] C. Ling, On the stresses in a notched plate under tension, J. Math. Phys. 26 (1947) 284–289, https://doi.org/10.1002/sapm1947261284.
[26] C. Ling, On stress concentration at semicircular notch, J. Appl. Mech. 34 (1964) 522–523, https://doi.org/10.1115/1.3607726.
[27] M. Leven, M. Frocht, Stress-concentration factors for single notch in flat bar in pure and central bending, J. Appl. Mech. 19 (1952) 560–561, https://doi.org/10.1115/1.4010559.
[28] P. Lazzarin, M. Zappalorto, J. Yates, Analytical study of stress distributions due to semi-elliptic notches in shafts under torsion loading, Int. J. Eng. Sci. 45 (2–8) (2007) 308–328, https://doi.org/10.1016/j.ijengsci.2007.04.007.

[29] M. Zappalorto, P. Lazzarin, J. Yates, Elastic stress distributions for hyperbolic and parabolic notches in round shafts under torsion and uniform antiplane shear loadings, Int. J. Solids Struct. 45 (18–19) (2018) 4879–4901, https://doi.org/10.1016/j.ijsolstr.2008.04.020.
[30] P. Romanowicz, B. Szybinski, M. Wygoda, Application of DIC method in the analysis of stress concentration and plastic zone development problems, Materials 13 (16) (2020) 3460, https://doi.org/10.3390/ma13163460.
[31] K. Golubiatnikov, A. Ghimire, F. Wald, M. Vild, Limit strain in the elastic-plastic, in: Nordic steel construction conference 2024, Stockholm: the swedish institute of steel construction, 2024, https://doi.org/10.5281/zenodo.11449395.
[32] K. Golubiatnikov, A. Ghimire, F. Wald, V. Stančík, Determination of design plastic strain limit for notched structural steel tensile specimens, Alex. Eng. J. 121 (2025) 38–52, https://doi.org/10.1016/j.aej.2025.02.075.
[33] H. Snijder, R. Dekker, P. Teeuwen, Net cross-section failure of steel plates at bolt holes: numerical work and statistical assessment of design rules, Eurosteel 1 (2–3) (2017) 3679–3688, https://doi.org/10.1002/cepa.424, ce/papers.
[34] EN 1990, Eurocode - Basic of Structural Design, Second edition, Brussels, 2002.
[35] FprEn 1993-1-14, *Design of steel structures — Part 1–14: Design assisted by finite element analysis.* Berlin, 2025.
[36] H. Snijder, D. Ungerman, J. Stark, G. Sedlacek, F. Bijlaard, A. Hemmert-Halswick, Evaluation of test results on welded connections in order to obtain strength functions and suitable model factors, in: *Part A: Results.* Background Documentation 6.05, 1988, pp. BI-88–139. Delft.
[37] H. Snijder, D. Ungerman, J. Stark, G. Sedlacek, F. Bijlaard, A. Hemmert-Halswick, *Evaluation of test results on welded connections in order to obtain strength functions and suitable model factors, Part B: Evaluation.* Background Documentation 6.06, BI-88-139. Delft, 1988.
[38] EN 1993-1-8, *Design of steel structures — Part 1–8: Design of joints.* Brussels, 2005.
[39] H. Snijder, B. Jitske, J. Maljaars, P. Teeuwen, Safety assessment for capacity design of bolted steel connections in tension, SDSS 5 (4) (2022) 282–289, https://doi.org/10.1002/cepa.1757, ce/papers.
[40] F. Sinur, D. Beg, Reliability analysis of net cross-section resistance with accidental eccentricity of holes, Steel Structures 9 (2009) 153–160, https://doi.org/10.1007/BF03249490.
[41] P. Može, Bearing strength at bolt holes in connections with large end distance and bolt pitch, J. Constr. Steel Res. 147 (2018) 132–144, https://doi.org/10.1016/j.jcsr.2018.04.006.
[42] P. Može, D. Beg, A complete study of bearing stress in single bolt connections, J. Constr. Steel Res. 95 (2014) 126–140, https://doi.org/10.1016/j.jcsr.2013.12.002.
[43] P. Hradil, A. Talja, Ductility Limits of High Strength Steels, Report VTT-R-04741-16., VTT Technical Research Centre of Finland, Espoo, 2016.
[44] S. Kim, C. Lee, S. Han, J. Wardenier, Deformation and strain limits for IPB-loaded high strength steel CHS joints, Thin-Walled Struct. 179 (2022) 109681, https://doi.org/10.1016/j.tws.2022.109681.
[45] I. Ryu, S. Kim, C. Lee, Experimental testing and plastic strain analysis of high strength steel longitudinal plate to tubular X joints, Thin-Walled Struct. 206 (2025) 112573, https://doi.org/10.1016/j.tws.2024.112573.
[46] W. Solonick, Elastic-Plastic Strain Acceptance Criterion for Structures Subject to Rapidly Applied Transient Dynamic Loading, Report KAPL-P-000034 (K96014)., KAPL Atomic Power Laboratory, New York, 1996.
[47] K. Golubiatnikov, M. Vild, F. Wald, A numerical-analytical prediction of the net cross-section resistance of weakened tensile plates, Preprint. Available at SSRN, https://ssrn.com/abstract=5491159, *2025*, https://doi.org/10.2139/ssrn.5491159.
[48] EN 10029, Hot-Rolled Steel Plates 3 Mm Thick or above - Tolerances on Dimensions and Shape, Brussels, 2010.
[49] ISO 6892–1, Metallic Materials - Tensile Testing, Part 1: Method of Test at Room Temperature, Geneva, 2009.
[50] L. Da Silva, L. Marques, T. Tankova, C. Rebelo, U. Kuhlmann, A. Kleiner, J. Spiegler, H. Snijder, R. Dekker, V. Dehan, A. Taras, C. Haremza, L. Cajot, O. Vassart, N. Popa, Standardization of Safety Assessment Procedures across Brittle to Ductile Failure Modes (SAFEBRICTILE), Directorate-General for Research and Innovation, European Commission, *Final report.* Luxembourg, 2015.
[51] X. Yun, L. Gardner, Stress-strain curves for hot-rolled steels, J. Constr. Steel Res. 133 (2017) 36–46, https://doi.org/10.1016/j.jcsr.2017.01.024.
[52] I. Faridmehr, M. Osman, A. Adnan, A. Nejad, R. Hodjati, M. Azimi, Correlation between engineering stress-strain and true stress-strain curve, Am. J. Civil Eng. Architect. 2 (1) (2014) 53–59, https://doi.org/10.12691/ajcea-2-1-6.
[53] EN 1090–2, Execution of Steel Structures and Aluminium Structures - Part 2: Technical Requirements for Steel Structures, Brussels, 2018.
[54] A. Sadowski, J. Rotter, T. Ummenhofer, On recent characterisations of the post-yield properties of structural carbon steels, Eurosteel 1 (2–3) (2017) 3577–3583, https://doi.org/10.1002/cepa.413, ce/papers.
[55] N. Agostoni, G. Ballio, C. Poggi, Statistical analysis of the mechanicalproperties of structural steel, Costruzioni Metalliche 2 (1993) 31–39.
[56] I. Arrayago, K. Rasmussen, E. Real, Statistical analysis of the material, geometrical and imperfection characteristics of structural stainless steels and members, J. Constr. Steel Res. 175 (2020) 106378, https://doi.org/10.1016/j.jcsr.2020.106378.
[57] P. Janas, M. Krejsa, V. Krejsa, Artists, *Structural reliability assessment using a direct determined probabilistic calculation*, in: Proceedings of the twelfth international conference on civil, structural and environmental engineering computing 72, Stirlingshire: Civil-Comp Press, 2009, https://doi.org/10.4203/ccp.91.72.
[58] L. Da Silva, T. Tankova, L. Marques, U. Kuhlmann, A. Kleiner, J. Spiegler, H. Snijder, A. Dekker, A. Taras, N. Popa, Safety assessment across modes driven by plasticity, stability and fracture, Eurosttel 1 (2–3) (2017) 3689–3698, https://doi.org/10.1002/cepa.425, ce/papers.